ELSEVIER

Atmospheric Research 33 (1994) 283–308

ATMOSPHERIC RESEARCH

A three-dimensional atmospheric radiative transfer model based on the discrete-ordinates method

A. Sánchez[1], T. F. Smith[2], W. F. Krajewski

Department of Mechanical Engineering, The University of Iowa, Iowa City, IA 52242, USA

(Received January 10, 1993; revised and accepted June 4, 1993)

Abstract

A three-dimensional, radiative transfer model based on the discrete-ordinates method for application to atmospheric radiation and remote sensing is developed. The model has the capabilities to address one-, two- and three-dimensional rectangular parallelepiped geometries containing nonhomogeneous, absorbing, emitting, anisotropically scattering media. Various boundary conditions including collimated and isotropic radiant sources are incorporated in the model. Where possible, the model takes advantage of symmetric and periodic boundary conditions to reduce the size of the solution domain. The model yields the radiant intensity field as a function of spatial location and direction within the solution domain and for any outward going direction. The model is extensively validated for one-, two- and three-dimensional geometries. The validation is performed through comparison of results from the model against those in the literature. Broken-cloud intensity fields are presented to demonstrate the capabilities of the model.

1. Introduction

Earth's energy balances, global circulation patterns, and climatic variations are examples of studies in which quantitative understanding requires modeling of the three-dimensional aspects of atmospheric radiation. Proper interpretations of satellite sensed data of radiant intensity for extraction of information related to cloud properties, ground temperature and rainfall require a radiative transfer model. Current interests in atmospheric energy balances and the role of clouds in affecting climatic changes provide additional impetus for developing a detailed

[1]Presently Escuela de Ingeniería Mecánica, Universidad de los Andes, Mérida, Edo, Mérida, Venezuela.
[2]To whom all correspondence should be sent.

SSDI 0169-8095(93)E0088-G

three-dimensional atmospheric radiative transfer model. The need for such a model is further emphasized by the atmospheric radiation measurements and modeling program (DOE 1990a, b) and planned satellite missions of tropical zone radiation and rainfall observations (Simpson et al., 1988).

Three-dimensional models of atmospheric radiative transfer are limited. Studies of radiative properties of broken cloud fields (Stephens, 1988; Kobayashi, 1989; Welch and Wielicki, 1989) are examples where three-dimensional effects have been considered. Most of the work cited used the Monte Carlo approach or an extensive mathematical formulation for solving the radiative transfer problem. Passive microwave modeling of convective clouds and rainfall (Mugnai et al., 1990; Adler et al., 1991) considered three-dimensional cloud structures but only one-dimensional radiative transfer. Despite the availability of these studies, much more effort is required before a quantitative understanding of large-scale radiative transfer problems of practical interest is acquired. Development of a comprehensive radiative transfer model is a necessary step towards this goal.

The objective of this paper is to present a three-dimensional atmospheric radiative transfer model capable of handling nonhomogeneous, anisotropic scattering atmospheres with a variety of radiation boundary conditions including a collimated radiant source. The model allows for calculating the outgoing intensity in any direction and, therefore, is suitable for remote sensing studies. In addition, the divergence of the radiative flux is also calculated, thereby allowing the model to be interfaced with other energy transfer studies. The model is based on the discrete-ordinates method. The capabilities of the model are demonstrated through a simulation of a sensor-observed broken cloud field.

The formulation of the model is presented in Section 2 and the solution methodology is discussed in Section 3. Validation and testing of the model is described in Section 4. Application of the model to the simulation of radiative transfer in a broken cloud field is presented in Section 5. Conclusions and recommendations for future studies are given in Section 6.

2. Governing equations

The intent of this discussion is to present the continuous forms of the governing equations in order to illustrate the type of equations being solved by the numerical model. The equations consist of the divergence of the radiative flux, the radiative transfer equation for the radiant intensity, and the boundary conditions. Due to the spectral variation of the radiative properties and the energy terms, an integration over all wavelengths must be accounted for. Also, directional effects for the radiant intensity must be included. Spatial variations of the radiant properties and energy terms are also allowed. The section concludes with a brief discussion of the radiative properties appearing in the governing equations.

2.1. Divergence of radiative flux

The divergence of the radiative flux appears in the energy balance as the net

radiant energy leaving a control volume per unit volume and represents the difference between the emitted radiant energy and the absorbed irradiation. Special attention must be given to the possibility that a collimated radiant source may irradiate the medium at a boundary. Because of the strong directionality of a collimated beam, it is advantageous to account for the collimated beam separately as it passes through the medium. The collimated source is located in the direction $\bar{\omega}_c$. The divergence of the radiative flux is expressed as:

$$\nabla \cdot \bar{q}_r = 4 \int_0^{\infty} a_\lambda \left[\pi I_{b\lambda} - \int_0^{4\pi} I_\lambda(\bar{\omega}) \, d\omega - I_{c\lambda} \right] d\lambda \tag{1}$$

where a_λ is the spectral absorption coefficient with λ denoting wavelength, $I_{b\lambda}$ is the spectral blackbody intensity evaluated using Planck's law, I_λ is the spectral radiant intensity for the $\bar{\omega}$-direction, ω is the solid angle, and $I_{c\lambda}$ is the direct intensity at the considered position due to a collimated radiant source at the medium boundary. The dependency of a_λ, $I_{b\lambda}$, and I_λ on the spatial variables is understood. In view of Eq. (1), an expression for the spectral radiant intensity for all directions within a spherical space around the control volume is needed.

2.2. The equation of transfer

The propagation of radiation along a line-of-sight direction ζ is described by the radiative transfer equation. For unpolarized radiation, the change in the radiant intensity $I(\zeta)$ in the $\bar{\omega}_c$ direction is expressed by the radiative transport equation stated by:

$$dI/d\zeta = -\beta I(\zeta) + S(\zeta) \tag{2a}$$

where the radiation source function is:

$$S(\zeta) = aI_b + \frac{s}{4\pi} \int_0^{4\pi} I(\zeta, \bar{\omega}_i) \, \Phi(\bar{\omega}_i, \bar{\omega}) \, d\omega_i + \frac{s}{4\pi} I_c(\zeta) \, \Phi(\bar{\omega}_c, \bar{\omega}) \tag{2b}$$

The wavelength dependence of all radiant energy and property quantities is understood. In Eq. (2), β is the extinction coefficient given by the sum of the absorption coefficient and scattering coefficient s, Φ is the scattering phase function for radiant energy incident within solid angle ω_i about the $\bar{\omega}_i$-direction and scattered into solid angle ω about the $\bar{\omega}$-direction. Physically, the terms on the right-hand side of Eq. (2a) represent attenuation of the intensity due to absorption and outward scattering and the enhancement of the intensity due to emission and inward scattering. The scattering phase function is normalized such that:

$$\frac{1}{4\pi} \int_0^{4\pi} \Phi(\bar{\omega}_i, \bar{\omega}) \, d\omega = 1 \tag{3}$$

The boundary condition for Eq. (2) consists of specifying the intensity at $\zeta=0$. The boundary intensities are discussed in Section 2.3. In terms of a collimated intensity at $\zeta=0$, the direct intensity at location ζ is:

$$I_c(\zeta)=I_c(0)\ e^{-\tau} \tag{4}$$

where $I_c(0)$ is the direct intensity at the boundary. The optical thickness from the boundary to the location under consideration is defined as:

$$\tau=\int_0^{\zeta}\beta\,d\zeta^* \tag{5}$$

The sensed intensity as measured by a radiant sensor placed at ζ is the sum of the intensity from Eq. (2) plus the direct intensity from Eq. (4) and is expressed by:

$$I_s(\zeta)=I(\zeta)+\delta(\bar{\omega}-\bar{\omega}_c)\ I_c(\zeta) \tag{6}$$

where δ is the Dirac delta-function. By Eq. (6), the direct intensity is only added when the sensed intensity is sought for the direction $\bar{\omega}=\bar{\omega}_c$.

2.3. Boundary conditions

The boundary condition for the radiant intensity at any given boundary and for the $\bar{\omega}$-direction can be expressed as:

$$I^+=\epsilon I_b^+ +\tau_s[I_{ba}^o+\delta(\bar{\omega}-\bar{\omega}_c)I_c^o]+\frac{\rho_d}{\pi}f_d\left[I_c^- +\int_0^{2\pi} I^-(\bar{\omega}^-)\eta\,d\omega^-\right] +\rho_d(1-f_d)I_m^- \tag{7}$$

In Eq. (7), superscripts +, −, and o indicate radiation going from the boundary toward the medium inside the domain, from the medium toward the boundary, and from outside the domain toward the boundary, respectively. The boundary has an emittance ϵ and blackbody intensity I_b^+, which depends on the temperature of the boundary surface. The transmittance and reflectance of the boundary are denoted by τ_s and f_d respectively, which, for convenience, are taken to be independent of direction. The fraction of the reflection that is diffuse is f_d. The diffuse background radiation is I_{ba}. The cosine of the angle between the direction of propagation of I^- and the normal to the given boundary is η. The intensity in the direction mirroring the direction of I^+, that is the specularly reflected intensity, is I_m^-. This mirrored intensity also includes the direct intensity that experiences specular reflection into the $\bar{\omega}$-direction. Physically, the terms on the right-hand side of Eq. (7) represent emission, transmission of diffuse and direct intensities from outside of the medium, diffuse reflection of incident intensity from within the medium and of direct intensity from another boundary location (multiple collimated radiant sources may exist), and specular reflection of incident intensity. The expression in Eq. (7) could be modified to account for

bidirectional reflectance and transmittance distribution functions. The intensities of I_b^+, I_{ba}°, I_c° and I_c^- are assumed known.

2.4. Radiative properties

The radiation equations require, for their solution, knowledge of the radiative properties of both the medium and the boundaries. In particular, the extinction and absorption coefficients of the medium as well as the scattering phase function (for scattering media) must be known. As indicated by Eq. (7), the radiative properties of the boundary consist of the emittance, reflectance, and the fraction of the reflectance that is diffuse. For the present study, interest is focused on absorbing, emitting, and scattering particles, not necessarily of the same composition and phase.

Under the assumption that the distance between the individual particles, considered as spheres, is much greater than the incident wavelength, it is possible to study the radiative properties of a single particle without reference to the other ones. The extinction and scattering cross-sections as well as the phase function for the scattering of electromagnetic waves by a single spherical particle are available (Bohren and Huffman, 1983). The cross-sections depend on the wavelength of interest, the particle radius, and the complex refractive index of the substance under consideration. The complex refractive index is expressed in terms of refractive and absorptive indices (optical constants) and depends on the incident wavelength as well as the temperature and composition of the particles. Polydispersions of particles are typically characterized by a function describing the particle size and number distribution $n(r)$, where r is the particle radius.

Radiative properties of a polydispersion are found by integrating the radiative properties of the individual particles over the size distribution. This is accomplished by means of the expression:

$$\chi = \int_{r_{min}}^{r_{max}} \sigma_\chi(r)\, n(r)\, \mathrm{d}r \tag{8}$$

where χ represents either the extinction, scattering, or absorption coefficient for the polydispersion, and σ_χ are the corresponding cross-sections for a single particle. The phase function for a scattering angle θ is calculated from:

$$\Phi(\theta) = \frac{1}{S} \int_{r_{min}}^{r_{max}} \sigma_{sca}(r)\, \Phi(\theta, r)\, n(r)\, \mathrm{d}r \tag{9}$$

Information for the optical constants and the particle size distribution is required, but is not always available. Also, calculations for scattering-phase functions for large (relative to wavelength) spherical particles can be very tedious, and computationally expensive. As a result of these drawbacks, approximate phase functions are commonly used in the simulation and parameterization of physi-

cally-based problems. Expressions for some of these phase functions are described later.

3. Solution methodology

The objective of this work is to develop a radiative transfer model that, based on the governing equations cited in Section 2, could be applied to a wide variety of atmospheric radiation studies including cloud radiation and remote sensing applications. This implies that the procedure used to solve the governing equations must (i) provide the radiant intensities and the divergence of the radiative flux; (ii) be capable of handling multi-dimensional systems including being able to be reduced to a smaller dimensional problem; (iii) account for parallel beam radiation and a wide variety of radiation boundary conditions; (iv) account for absorbing, emitting, and anisotropically scattering and nonhomogeneous media with wavelength and temperature dependent properties; and (v) be compatible with other energy transfer mechanisms. Additionally, the method must be computationally efficient, accurate, and stable and should have the potential to take advantage of contemporary computer designs based on vectorization and parallelization. Of the various methods for solving the governing equations, the discrete-ordinates method has the capabilities to satisfy these requirements.

3.1. The discrete ordinates method

Several authors have presented formulations of the discrete-ordinates method (Carlson and Lathrop, 1968; Gerstl and Zardecki, 1985; Fiveland, 1988; Fiveland and Jamaluddin, 1991; Kim and Lee, 1989; Sánchez, 1991). These references should be examined for details regarding the derivation of the discrete-ordinates method. For the presentation here, the discretized form of the radiative transfer equation is given first. The entire three-dimensional domain is subdivided into cubical control volumes as shown in Fig. 1 where control volume P with differential volume $\Delta V = \Delta x \Delta y \Delta z$ is of interest. Control volume P is surrounded by six adjacent control volumes labeled W (west), E (east), S (south), N (north), F (front) and B (back) with associated interfaces of w, e, s, n, f and b. In addition to the spatial discretization, the direction of propagation of the radiant intensity is also discretized. Each control volume is homogeneous, and nonhomogeneities are accounted for by assigning different radiative properties to the control volumes. For control volume P, the derivatives in Eq. (2) are replaced by their finite difference approximation and both sides of the equation are integrated over ΔV. Extrapolated intensities are introduced to yield the intensity at control volume P for discrete direction i as:

$$I_i^P = \left(\frac{\mu_i}{\Delta x} I_i^{x\mathrm{r}} + \frac{\delta_i}{\Delta y} I_i^{y\mathrm{r}} + \frac{\gamma_i}{\Delta z} I_i^{z\mathrm{r}} + \alpha(S_{1i}^P + S_{2i}^P + S_{3i}^P)\right) \times \left(\frac{\mu_i}{\Delta x} + \frac{\delta_i}{\Delta y} + \frac{\gamma_i}{\Delta z} + \alpha\beta\right)^{-1} \tag{10}$$

where the direction cosines μ_i, δ_i, and γ_i are for the x, y and z directions, respectively. Selection of the discrete directions is discussed later. Superscripts r designate the interface from which the radiant energy originates for the indicated coordinate. Selection of the interpolation weighting factor α is discussed in Section 3.4. The intensities arriving at the end-faces (which become the reference intensities for the neighboring control volumes) are recovered from:

$$I_i^{x\mathrm{e}} = [I_i^P + (\alpha - 1) I_i^{x\mathrm{r}}]/\alpha \tag{11}$$

Expressions for $I_i^{y\mathrm{e}}$ and $I_i^{z\mathrm{e}}$ can be written by replacing x with y and z. In Eq. (10), S_{1i}^P, S_{2i}^P, and S_{3i}^P are the radiant sources for thermal emission, inward scattering, and collimated source, respectively, and are evaluated from:

$$s_{1i}^P = aI_\mathrm{b}, \tag{12a}$$

$$S_{2i}^P = \frac{s}{4\pi} \sum_{j=1}^{K} w_j I_j^P \Phi_{ij} \tag{12b}$$

and

$$S_{3i}^P = sI_\mathrm{c}^P \Phi_{i\mathrm{c}}/4\pi \tag{12c}$$

where K represents the number of discrete directions in a spherical space, w_j is

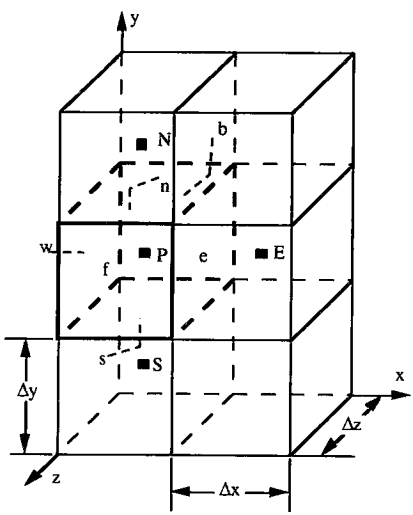

Fig. 1. Control volumes.

the angular quadrature weight associated with the incoming j direction, and Φ_{ij} is the phase function for scattering between the i and j discrete directions.

From Eq. (7), the boundary conditions for Eq. (10) are given by:

$$I_i^+ = \epsilon I_b^+ + \tau_s[I_{ba}^o + \delta(\bar{\omega}_i - \bar{\omega}_c)I_c^o] + \frac{\rho_d}{\pi} f_d \left[I_c^- + \sum_{j=1}^{K/2} w_j \eta_j I_j^- \right] + \rho_d (1 - f_d) I_m^- \tag{13}$$

where η_i is the cosine of the angle between the normal to the surface (boundary) and the direction of propagation j. It should be recognized that the summation in Eq. (13) is over only the four octants above a boundary that lie within the medium.

Eqs. (10) and (13) are formulated for a single wavelength. To account for the spectral variation of radiative properties, an integration over the entire spectrum as indicated in Eq. (1) is needed. To this end, the spectrum is discretized into W rectangular wavelength bands, where the radiative properties, evaluated at the discrete wavelength (λ) corresponding to the center of each band, are assumed constant over each band. Integrated quantities are found as the summation over all bands of the individual contributions for each band. This treatment of the spectral problem is based on a noncorrelated, nongray gas analysis (Fiveland and Jamaluddin, 1991; Kim et al., 1991), which implies that intensities and radiative properties, averaged over a wavenumber interval, are considered independent of each other. This approach to the spectral problem represents a good compromise between accuracy and computational time, particularly when rapid variations of temperature and radiative properties with wavelength are not expected (Kim et al., 1991). The method for performing the wavelength integration is illustrated using:

$$\int_0^\infty \chi_\lambda I_\lambda \, d\lambda = \sum_{\lambda_i=1}^{W} \bar{\chi}_{\lambda_i} \bar{I}_{\lambda_i} \Delta\lambda_i \tag{14}$$

where χ is representative of any radiative property and the overbar indicates that it is band averaged. The average intensity $\bar{I}_{\lambda_i}$ is the average of I_λ over the wavelength interval $\Delta\lambda_i$. If the medium contains absorbing and emitting gases, then the k-distribution method could be utilized (Fu and Liou, 1992).

The total divergence of the radiative flux as stated in Eq. (1) for control volume P is evaluated from:

$$\nabla \cdot \bar{q}_r^P = \sum_{\lambda_i=1}^{W} \left[a_{\lambda_i} \left(4\pi I_{b\lambda_i}^P - \sum_{j=1}^{K} w_j I_{j\lambda_i} - I_{c\lambda_i}^P \right) \right] \tag{15}$$

The heat flux at any given surface k becomes:

$$q_k = \sum_{\lambda_i=1}^{W} \left(I_{c\lambda_i}^- \eta_c + \sum_{j=1}^{k/2} w_j \eta_j I_{j\lambda_i} \right) \tag{16}$$

An energy balance for the solution domain states that the radiant energy entering equals the radiant energy leaving and is used as one means for verification of the solutions.

The solutions for the radiant intensity were obtained using an iterative process. For a given direction, scans are made for each coordinate. These scans are repeated for each direction. This is repeated until convergence is reached.

3.2. Selection of a quadrature set

A quadrature set has been used to replace the integrals contained in the governing equations by summations. The choice of quadrature for the discrete-ordinate method is not unique but several restrictions are placed on the set (Carlson and Lathrop, 1968; Fiveland, 1991; Sánchez and Smith, 1992). The so-called "Level Sequential-Odd Quadrature" is used in this work. The discrete ordinates are referred to as S-N, where the total number of directions is:

$$K=N(N+2) \tag{17}$$

Quadrature sets for any value of N were generated from a computer code and agree with those listed by Fiveland (1991).

3.3. Modeling the phase function

For energy to be conserved, the quadrature set must integrate accurately the scattered intensities, that is, the terms of $w_j I_j \Phi_{ij}$ in Eq. (12), for all forms of phase functions. Because the integration procedure has already been selected, the phase function may need modifying in order to guarantee conservation of energy. Eq. (3) states that the phase function is normalized if energy is to be conserved. Because only discrete values of $\Phi(\omega_j,\omega_i)$ are evaluated, the integration in Eq. (3) is performed numerically using:

$$\frac{1}{4\pi}\sum_{i=1}^{K}\Phi_{ij}w_i=1 \tag{18}$$

An accurate integration procedure results from expanding the phase function in a series of Legendre polynomials $P_n(\cdot)$ as follows:

$$\Phi_{ij}=\sum_{n=0}^{M_1}(2n+1)b_nP_n(\cos\theta_{ij}) \tag{19}$$

where M_1 represents the number of terms in the series, b_n are coefficients for the series expansion of the phase function in terms of Legendre polynomials of order n, and the cosine of the angle between discrete directions i and j is evaluated from:

$$\cos\theta_{ij}=\mu_i\mu_j+\delta_i\delta_j+\gamma_i\gamma_j \tag{20}$$

The representation of the phase function in terms of Legendre polynomials al-

lows for the accurate evaluation of this function between any two directions based on known discrete values.

When a quadrature set is used in the integration of Eq. (19), energy conservation may not be satisfied for values of N that yield reasonable computational times. To address this concern, the renormalized phase function $\bar{\Phi}_{ij}$ is:

$$\bar{\Phi}_{ij}=\Phi_{ij}\Big/\frac{1}{4\pi}\sum_{i=1}^{K} w_i \Phi_{ij} \,. \tag{21}$$

An isotropic phase function ($\Phi=1$) does not require renormalization. In the remainder of this work, the overbar indicating a renormalized phase function is omitted for simplicity; it is understood, however, that the phase functions are always renormalized.

For highly anisotropically scattering particles (large rain droplets, for example), Eq. (19) may require an excessive number of terms in order to describe accurately the phase function. To address this concern, the phase function is scaled using the δ–M scaling method (Wiscombe, 1977; Kim and Lee, 1990a). In the δ–M scaling, the original phase function Φ is replaced by a forward term and a scaled scattering phase function $\tilde{\Phi}$:

$$\Phi_{ij}=4\pi f\delta'(\bar{\omega}_i-\bar{\omega}_j)+(1-f)\tilde{\Phi}_{ij} \tag{22}$$

where f is a forward fraction parameter to be defined later, δ' is the Kroneker delta-function, and the tilde indicates a scaled quantity. When Eq. (22) is substituted into Eq. (2) and the following scaled properties are introduced:

$$\tilde{s}=s(1-f) \tag{23a}$$

$$\tilde{\beta}=\beta-fs \tag{23b}$$

an expression identical to the form of Eq. (2) results with the radiative properties of s and β replaced by the respective scaled properties in Eq. (23). Hence, the numerical formulation of the discrete-ordinates method does not have to be modified provided the scaled radiative properties are used. From Eq. (5), the optical thickness of the scaled domain is less than that with unscaled properties. The scaled phase function in Eq. (22) is expanded in a series of Legendre polynomials:

$$\tilde{\Phi}_{ij}=\sum_{n=0}^{M-1}(2n+1)\tilde{b}_n P_n(\cos\theta_{ij}) \tag{24}$$

where M (the number of terms in the scaled series) is less than M_1. The coefficient of the term where the original series is truncated (b_{M1}) is used to define the forward fraction parameter:

$$f=b_{M1} \tag{25}$$

Substituting Eqs. (24) and (19) into Eq. (22) and equating coefficients (up to the M term), the expression for the scaled coefficients $\tilde{b}_n$ is obtained:

$$\tilde{b}_n = \frac{b_n - f}{1 - f} \tag{26}$$

It should be remembered that the scaled phase function needs to be renormalized according to Eq. (21). The scaling method results in a transformation of a given optically thick, highly anisotropic problem into a similar one that is optically thinner and requiring fewer discrete directions for its solution. This transformation is, however, not free of possible complications. If the scaling is too ambitious (for example, applying a δ–M transformation (Wiscombe, 1977) with $M=4$ to a phase function that requires two hundred terms for its series expansion), the scaled phase function will produce physically unrealistic negative values.

In order to avoid negative values of the phase function, Kim and Lee (1990b) suggest to further modify the scaled phase function by adding a positive constant according to:

$$\hat{\Phi}_{ij} = \frac{\tilde{\Phi}_{ij} + B}{1 + B} \tag{27}$$

where B is the largest negative (if any) value taken by $\hat{\Phi}_{ij}$:

$$B = \max\left|\frac{\tilde{\Phi}_{ij} - |\tilde{\Phi}_{ij}|}{2}\right| \tag{28}$$

Equating the terms in the series of Legendre polynomials in Eq. (27), the coefficients for the expansion of the modified δ–M phase function are:

$$\hat{b}_n = \frac{\tilde{b}_n + B\delta'(n)}{1 + B} \tag{29}$$

The forward fraction parameter is defined as:

$$\hat{f} = \frac{(1+B)b_1 - \tilde{b}_1}{(1+B) - \tilde{b}_1} \tag{30}$$

In a procedure similar to that of the previous section, the radiative properties are found to be scaled by:

$$\hat{s} = \tilde{s}(1 - f) \tag{31a}$$

and:

$$\hat{\beta} = \tilde{\beta} - f\tilde{s} \tag{31b}$$

As before, the phase function from Eq. (27) requires renormalization.

3.4. Other features

The calculation of I_c^P in Eq. (12c) is based on some location within control volume P, which may not be at the center of control volume P. This location was obtained by spatially averaging the direct beam attenuation over the control vol-

ume. Assume that the direct beam is incident on the top of the system shown in Fig. 1. The distance measured from interface n where the direct intensity reaches its average value is:

$$\Delta y_P = \ln\left[\left(\frac{\beta\Delta y}{\delta_c[1-\exp(-\beta\Delta y/\delta_c)]}\right)^{\delta_c/\beta}\right] \tag{32}$$

Similar expressions apply for Δx_P and Δz_P by replacing δ_c and Δy with their counterparts. Values of Δx_P, Δy_P, and Δz_P are used to find ζ in Eq. (4) and the calculation of I_c^P in Eq. (12c).

In many applications, the radiation field presents periodicity in one or more directions. From the point of view of both memory requirements and computing time, it is advantageous to apply a "mirror technique between facing boundaries" to the directions of periodicity. Hence, the intensities going out of a surface (for a given iteration) are placed as intensities coming into the opposite wall (boundary condition for the next iteration) for the direction being modeled. Furthermore, the radiation field in some applications may have symmetry across a given plane in one or more directions. Planes of symmetry behave in a way similar to specularly reflecting walls. A "mirror technique" can be applied to the plane or planes of symmetry (or specularity). In this procedure, the intensities going out of a surface (for a given iteration and for the direction being modeled) are placed as intensities coming into the same wall (boundary condition for the next iteration) in the mirroring direction. It is important to notice that the symmetry requirement refers to the radiation field. In general, a collimated source will render this field non-symmetric and caution must be exercised.

The model has the capability to solve lower order dimensional problems (Sánchez et al., 1993). This capability allows for comparison and possible parameterization of predictions obtained using different dimensionalities in the solution of a given problem. An examination of the derivation of Eq. (10) reveals that the degree of dimensionality is dictated by the presence of the direction cosines and the phase function. A simple procedure to simulate lower dimensionalities by means of a general 3D code is to select the quadrature set, calculate the phase function for all pairs of directions (including, if present, beam and sensor), set the direction cosines in the direction (2D) or directions (1D) of "infinite" length to zero, and solve for the intensities.

In some applications, the intensity toward a satellite or sensor in directions other than those of the discrete quadrature set may be required. The intensities from Eq. (10) contain enough information to describe the entire radiation field and to evaluate the source terms (S_1, S_2, and S_3) required to apply Eq. (10) to any sensor direction (μ_s, δ_s, and γ_s). The set of discrete intensities I_i^P is known throughout the entire domain. The intensities in the direction of the sensor are calculated by evaluating the boundary intensities from Eq. (13), the source terms from Eq. (12), and then applying Eqs. (10) and (11) to obtain the desired output intensities. This procedure does not require interpolation between the discrete directions.

Assignment of the numerical value of the finite-difference weighting factor α (see Eq. 10) is based on the dimensionality of the problem. For one-dimensional systems, the procedure suggested by Fiveland and Jamaluddin (1991) is used. The procedure consists of initially setting $\alpha = 0.5$ and, if negative intensities are encountered, the value of α is increased until positive intensities are found or until $\alpha = 1$. For two- and three-dimensional problems, numerical experiments reveal that setting $\alpha = 1$ yields stable solutions and results that agree (see later sections) with those from other radiative transfer models.

Information about the computer code developed for implementing the discrete-ordinates method can be obtained from the authors.

4. Model validation and testing

The presented model and its numerical implementation was validated using several one-, two- and three-dimensional examples. For one-dimensional, atmospheric radiative transfer applications, an extensive source of published results is the comparative study by Lenoble (1985). The model was tested for a variety of situations discussed in Lenoble (1985). The tested scenarios included problems with walls and medium with spectrally dependent radiative properties, isotropic and anisotropic scattering, collimated beam, optically thick medium, and existence of a remote sensor to simulated the received intensities. For details of the test examples, an interested reader is refereed to Sánchez et al. (1992). Here, only one result for each of the one- and two-dimensional geometries is presented.

4.1. One-dimensional optically thick cloud

The test problem for the one-dimensional system is that proposed by the Radiation Commission (Lenoble, 1985) and concerns a thick atmosphere (roughly, a 4 km thick cloud) in the plane-parallel setting depicted in Fig. 2. The computations are carried out for a wavelength of 0.7 μm assigning a refractive index for

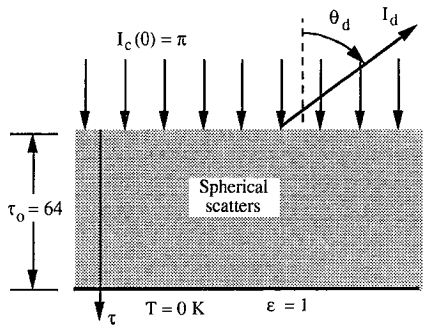

Fig. 2. Geometry used in the one-dimensional tests. Spherical scatters represent the C1 cloud and optical depth τ is measured from the top and varies from 0 to 64.

water of 1.33. For the case presented here, a detector output angle of 53.13° ($\delta_d=0.6$) is selected.

A polydispersion of type C1 is reported to have a drop size distribution resembling that found in real clouds. The C1 drop size distribution was used in the calculations (Deirmendjian, 1964; Lenoble, 1985). With these parameters, the cloud optical thickness is $\tau_o=64$ and the optical depth τ ranges from 0 to 64. To obtain an accurate solution for such a cloud, several layers would be required in the computational domain. Furthermore, a highly anisotropic scattering phase function is expected, due to the relative size of the wavelength under consideration and the range of the particle size in the polydispersion ($0.1 \leqslant r \leqslant 15$ μm). A modified δ-4 is used as discussed in Section 3.3 and the optical thickness is reduced to 1/3 of its original value (see Sánchez et al., 1992 for details).

The model computer implementation, called ANDISORD4, was run with a S-8 (40 streams up and 40 streams down) quadrature set and 10, 20, and 30 layers. The most sensitive results ($I_d(\tau)$ and $q_{net}(\tau)$ for intensity toward sensor and net flux at $\tau=0$, respectively) occur at the top surface of the layer. These results are displayed in Table 1 for single scattering albedo $\omega_o=s/\beta=1.0$. When the number of layers is increased from 20 to 30, the intensity toward the sensor increased by less than 0.4% while the net flux decreased by less than 1.5%. From Table 1, it can be concluded that, with 30 layers, the results are practically converged.

Tables 2 and 3 contain, for comparison, results for the sensor intensity I_d at

Table 1
Influence of the number of layers on the detector intensity and the net heat flux at the top of the cloud for the one-dimensional tests

Layers	$I_d(0)$	Change (%)	$q_{net}(0)$	Change (%)
10	0.8377	–	0.5207	–
20	0.8533	−1.86	0.4867	6.53
30	0.8566	−0.39	0.4799	1.40

Table 2
Intensity toward sensor for Cloud C1 as a function of optical depth for the one-dimensional tests.* ANDISORD4 is the current method and the other methods are described by Lenoble (1985)

Method	Intensity toward sensor ($\delta_d=0.6$)						
	$\tau=0$	$\tau=3.2$	$\tau=6.4$	$\tau=12.8$	$\tau=32$	$\tau=48$	$\tau=64$
Spherical harmonics	0.825	0.978	0.988	0.902	0.570	0.291	0.0
Finite difference	0.805	–	–	–	–	–	–
Monte Carlo	0.788	0.816	0.959	0.851	0.449	0.307	0.0
Asymptotic	0.821	–	1.010	0.901	0.568	0.292	0.0
ANDISORD4	0.857	0.977	0.989	0.908	0.575	0.294	0.0

*Underlined items denote interpolated values.

Table 3
Heat flux at top of cloud layer for Cloud C1 as a function of optical depth for the one-dimensional tests. ANDISORD4 is the current method and the other methods are described by Lenoble (1985)

Method	Net flux (direct+diffuse)						
	$\tau=0$	$\tau=3.2$	$\tau=6.4$	$\tau=12.8$	$\tau=32$	$\tau=48$	$\tau=64$
Spherical harmonics	0.4828 *	0.4826	0.4825	0.4825	0.4823	0.4822	0.4821
Finite difference	0.4811	0.4811	0.4811	0.4811	0.4811	0.4811	0.4811
Monte Carlo	0.4856	–	–	–	–	–	0.4856
Asymptotic	0.4900	–	0.5000	0.4950	0.4950	0.4950	0.4950
Discrete ordinates	0.4634	–	–	–	–	–	0.4633
Doubling	0.4796	0.4796	0.4796	0.4796	0.4796	0.4796	0.4796
Eddington	0.4731	0.4731	0.4731	0.4731	0.4731	0.4731	0.4731
Delta Eddington	0.4759	0.4759	0.4759	0.4759	0.4759	0.4759	0.4759
Standard Two streams	0.6703	0.6703	0.6703	0.6703	0.6703	0.6703	0.6703
Exponential kernel	0.4759	0.4759	0.4759	0.4759	0.4759	0.4759	0.4759
ANDISORD4	0.480	0.480	0.480	0.480	0.480	0.479	0.479

*Underlined items denote interpolated values.

$\delta_d=0.6$ and net radiative flux $q_{net}(0)$ obtained from this study using 30 layers and from several other methods reported by Lenoble (1985). Results provided by the present model are in good agreement with those of other methods. From the results presented in Tables 1 to 3, it can be seen that even the 10 layer system could have been used with approximately the same degree of accuracy.

4.2. Parallel beam radiation and isotropically scattering medium in a two-dimensional enclosure

The presented model is validated for two- and three-dimensional geometries using test problems that include isotropic and anisotropic participating media, black, gray, and highly reflecting walls, optically thick media, internal sources, radiative equilibrium, spectrally participating media, parallel beam at varied polar and azimuthal angles, and several types of boundary conditions (Sánchez et al., 1992). As an illustration, the problem of beam radiation incident on an isotropic medium in a two-dimensional enclosure is presented.

The geometry and the conditions for the problem modeled in this test are shown in Fig. 3. For the two-dimensional enclosure, the top wall is transparent, the other walls are opaque and black, and the length of the domain in the z-direction is infinite. The medium has unit optical thicknesses for the x- and y-directions and has $\omega_o=1.0$. Thermal emission of the walls and medium is neglected.

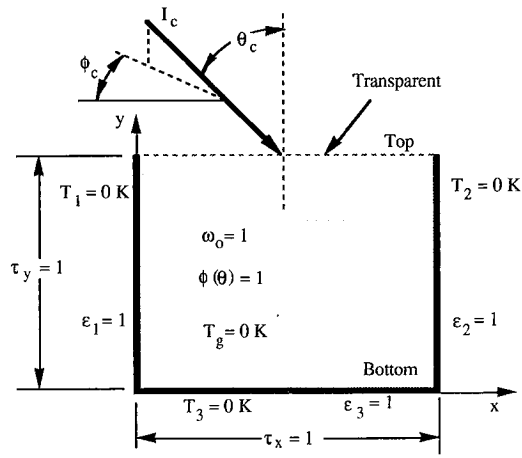

Fig. 3. Two-dimensional test geometry. The arrow labeled I_c denotes the direction of the collimated beam.

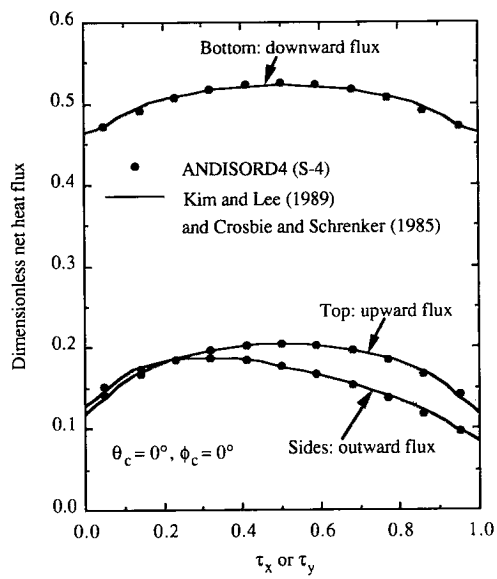

Fig. 4. Dimensionless heat fluxes for normal incidence for two-dimensional test problem.

Figs. 4 and 5 show comparisons of the results from the present model and those obtained by Crosbie and Schrenker (1985), Kim and Lee (1989), and Tan and Howell (1990) using two-dimensional models. In these figures, dimensionless heat fluxes are defined as the net fluxes divided by the heat flux at the top wall due to the parallel beam ($I_c \cos(\theta_c)$). In all the cases studied, the model is implemented on an 11×11 grid mesh, and a S-4 quadrature set is used. Especially

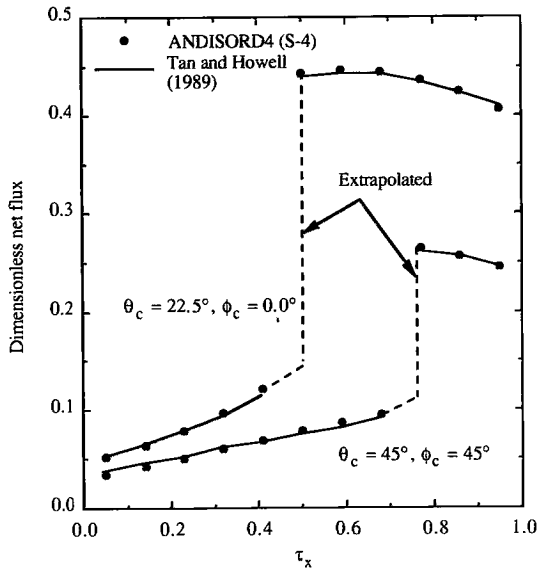

Fig. 5. Shadowing effects on the lower surface for the two-dimensional test problem.

significant is the good agreement with the results from Kim and Lee, considering that these authors used a discrete-ordinates model with a S-14 quadrature set and up to 25 non-uniform grid points. Excellent agreement is also obtained in the prediction of shadowing effects for those situations where the direction of the parallel beam is not perpendicular to the top surface (Fig. 5).

For three-dimensional geometries, the model is tested against engineering-type problems solved by Menguc and Viskanta (1985), Jamaluddin and Smith (1988), Naraghi et al. (1988), Truelove (1988), Fiveland and Jamaluddin (1991), Naraghi and Huan (1990) and Tan and Howell (1990). In all cases, the presented method performed well. Details of these comparisons are given by Sánchez et al. (1992).

The model capabilities are also tested by solving a number of additional problems (Sánchez et al., 1992). These problems include two- and three-dimensional coupling of radiative transfer model with models of other forms of energy transfer (including natural and forced convection); three-dimensional collimated source and sensor configurations at different angles and under different scattering conditions; three-dimensional, nonhomogeneous problems in optically thin and optically thick settings; and three-dimensional spectral problems including radiative equilibrium.

In the next section, results of the three-dimensional simulation of radiation by a broken cloud field is presented. Some of the calculated quantities can be compared directly with results obtained by Welch and Wielicki (1989) using a Monte Carlo method, whereas other results are original.

5. Broken cloud field simulation

Although the real shape of clouds can vary widely, and could be described by fractals (Mandelbrot 1983), semi-infinite geometries and cubical arrays have been commonly used by different investigators (McKee and Cox, 1976; Welch and Wielicki, 1989) to study the radiative characteristics and properties of clouds. Due to the complexities and physical dimensions of the problems considered, the Monte Carlo method has been commonly used for the solution of such problems. The intention of this example is to show that the three-dimensional model developed in this work can be used in the analysis of these problems.

5.1. Geometry

An infinite array of cubical clouds is shown in Fig. 6. The clouds have dimensions of $1\times1\times1$ km and are placed 1 km above a diffuse surface with an albedo of 0.3. The scattering of radiation by the cloud particles is represented by a Henyey–Greenstein phase function with an asymmetry parameter $g=0.86$. The cloud optical thickness is 10. Solar radiation irradiates the cold (non-emitting) clouds at a polar angle $\theta_c=60°$ and an azimuthal angle $\phi_c=0°$. The output of radiation measured by a satellite (with a very narrow field of view) placed at a location defined by a polar angle of 53.13° and a given azimuthal angle is evaluated.

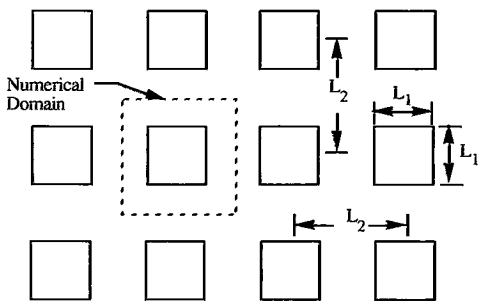

(a) Top view

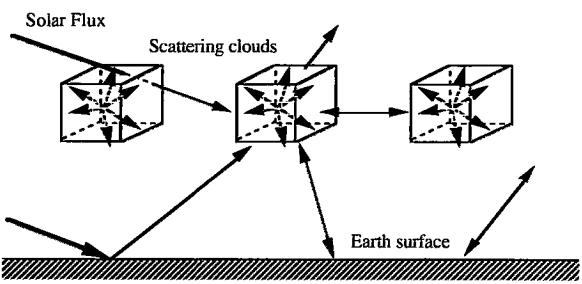

(b) Interactions

Fig. 6. Geometry for the infinite field of broken clouds.

5.2. Scattering albedo

Welch and Wielicki (1989) used a Monte Carlo method to evaluate the albedo of this cloud–space–earth configuration for different ground albedos, cloud optical thicknesses, and cloud cover. The cloud cover CC is defined as:

$$CC=(L_1/L_2)^2, \tag{33}$$

where L_1 and L_2 correspond to the dimensions indicated in Fig. 6.

The cloud cover is modified by changing the dimension L_1, while L_2 and the altitude of the clouds remains constant. The model is implemented with different grid configurations ranging from a $1\times10\times1$ uniform grid (for clear sky, $CC=0.0$ and, for all covered sky, $CC=1.0$) to an $11\times10\times11$ non-uniform grid (for $CC=0.9$) on the reduced numerical domain depicted in Fig. 6. This domain is formed by lateral periodic boundaries (notice, through, that the solar beam, with the shadows that it produces, renders the domain non-symmetric).

The computer code (Sánchez et al., 1992) has the built-in capability for evaluating Henyey–Greenstein phase functions for user-provided asymmetry parameters. For this type of application, with large optical thickness and highly anisotropic phase function, a "Henyey–Greenstein modified δ-4" option is selected. The original as well as the scaled phase functions resulting from these calculations are shown in Fig. 7. Note that the modified δ-4 model does not give as small of

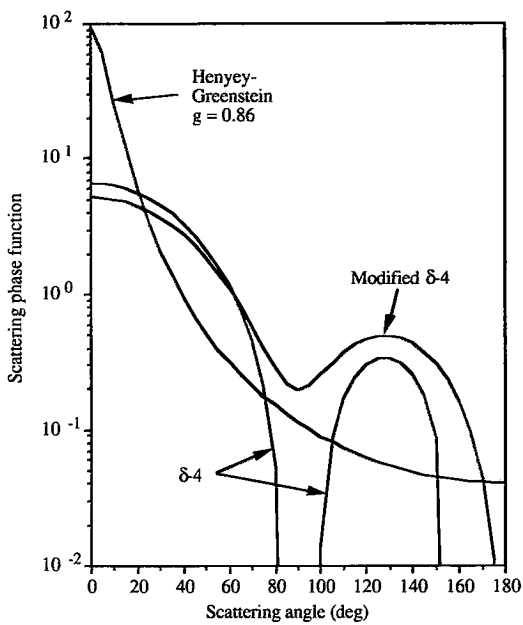

Fig. 7. Phase function for cubic cloud example.

values for the phase function for scattering angles near 90° and 180° as for the δ-4 model.

Cloud field albedos calculated with an S-8 implementation of the discrete-ordinates model for $\phi_c = 0°$ are compared in Fig. 8 with the corresponding values calculated by Welch and Wielicki (1989). An empirical parameterization (Welch and Wielicki, 1989) of the albedo based on the limiting values for clear sky (a) and the totally clouded sky (a_c) is also represented in the same figure. The results obtained with the model based on the discrete-ordinates method agree very well with those of Welch and Wielicki (1989). Equally good is the agreement between the empirically parameterized albedos and those calculated here. The parameterization, however, does not capture the behavior of the cloud field albedos in the region of intermediate cloud cover. The albedos proved to be very susceptible to the discretization in the vertical direction when the full three-dimensional problem, with periodic boundaries, is solved. In general, 10 layers in the vertical direction are needed.

5.3. Intensities

Dimensionless intensities (I/I_c) in the direction of the satellite are displayed in Figs. 9 and 10 for $CC = 0.36$. All the parameters in both figures are the same, with the exception of the satellite azimuthal angle, which corresponds to 0° for Fig. 9 and to 45° for Fig. 10. Evaluation of satellite sensed intensities is of importance for studies concerned with atmospheric remote sensing. The dimensionless intensities in Figs. 9 and 10 show the potential of the model. In these figures,

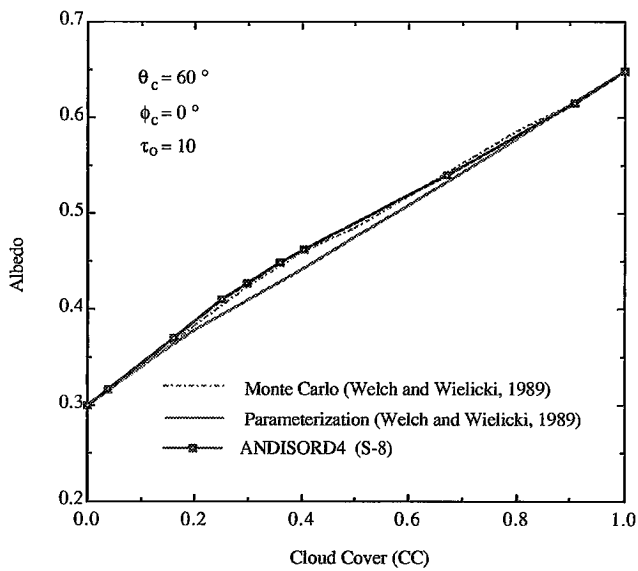

Fig. 8. Cloud field albedo estimates for ground albedo of 0.3 for the broken cloud field.

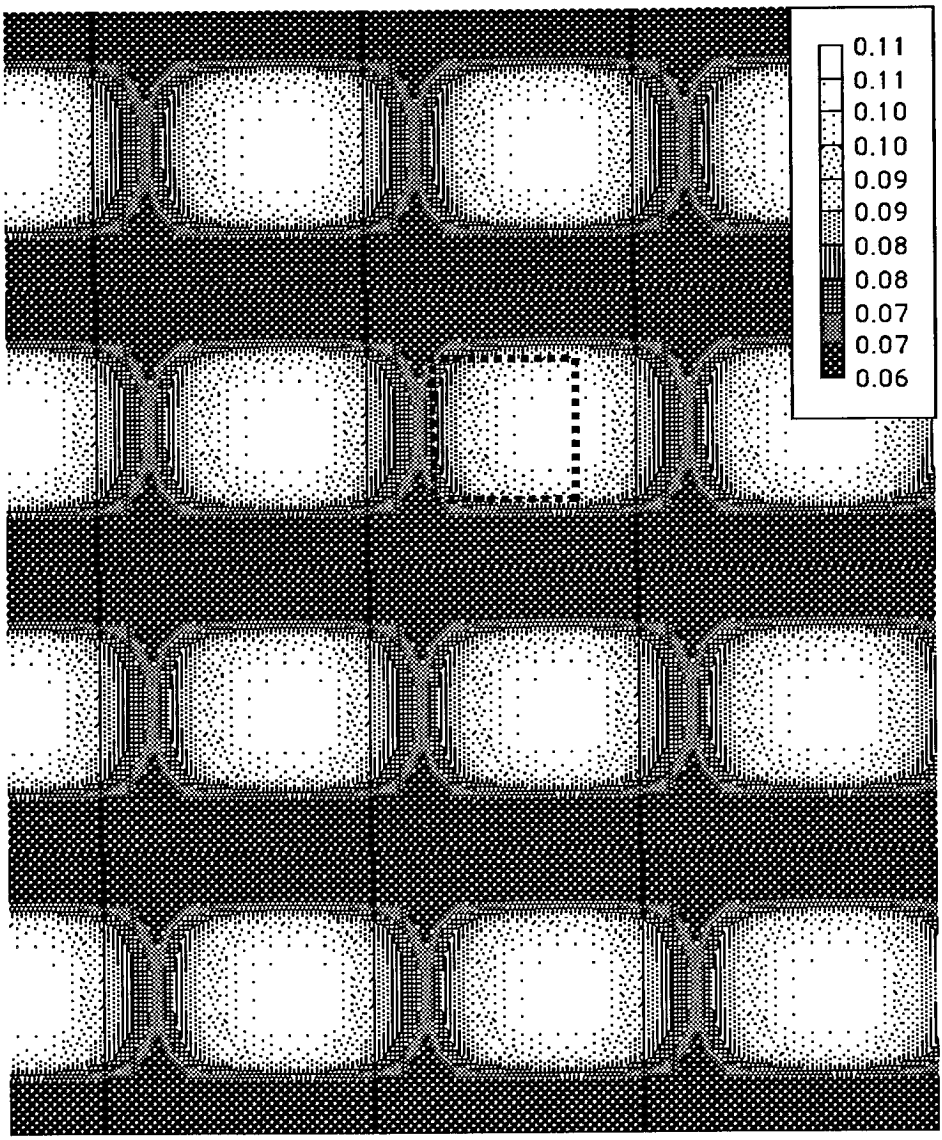

Fig. 9. Dimensionless intensities toward the satellite for ground albedo of 0.3 for the broken cloud field; $CC=0.36$; $\theta_c=60°$, $\phi_c=0°$; $\theta_d=53.13°$, $\phi_d=0°$.

the maximum intensity is always directed in the direction of the longest line of sight for the satellite. The original cubic clouds (represented by a dotted square in Figs. 9 and 10) are lost in the satellite image. Also, when comparing these two figures, it is evident that changing the relative position between the satellite and the other components of the system can drastically change the perceived image.

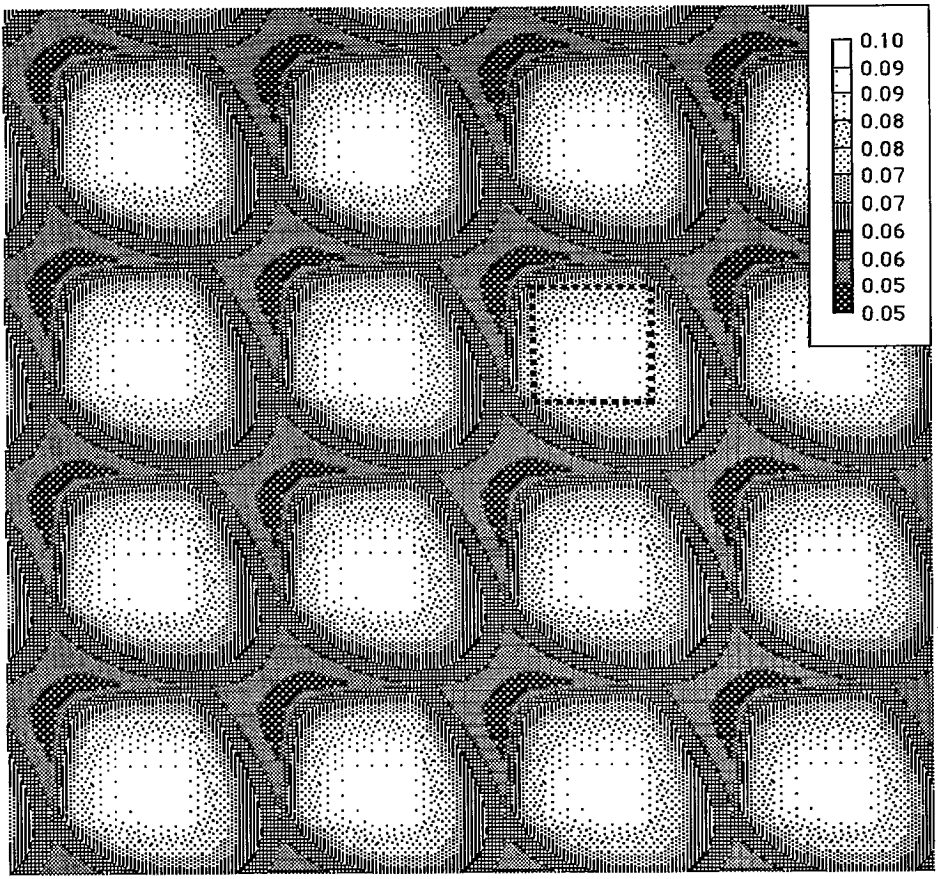

Fig. 10. Dimensionless intensities toward the satellite for ground albedo of 0.3 for the broken cloud field; $CC=0.36$; $\theta_c=60°$, $\phi_c=0°$; $\theta_d=53.13°$, $\phi_d=45°$.

The dimensionless solar intensity reflected by the ground is on the order of 0.048, which is not captured in either image. The "clear corridors" in Fig. 9 indicate a dimensionless intensity near 0.06 (compared with 0.048) indicating the interaction between the clouds and the ground.

6. Summary and conclusions

The development, implementation, and testing of a three-dimensional radiative transfer model for application to remote sensing in multidimensional systems containing spectrally participating scattering media are described. The capabilities of the discrete-ordinates method are the main reasons for its selection as the working tool for the model. The formulation based on the discrete-ordi-

nates method is used to develop a computational algorithm that takes advantage of the solution for the intensity field provided by the model. The algorithm is implemented in the form of a computer package (with components called ANDISORD4 and MDATOS) written in FORTRAN 77. The code has the following capabilities:

(1) Geometry: the model can solve for one-, two- and three-dimensional geometries.
(2) Media: the model is capable of treating nonhomogeneous, anisotropically scattering media in the presence of real gases and polydispersions.
(3) Optical range: the model is applicable for any range of optical thickness.
(4) Spectral range: the model can be used for a single wavelength, a selected band or the entire spectrum.
(5) Parallel beam radiation: the model can handle a collimated beam incident from any direction and on any set of surfaces.
(6) Boundary conditions: the model includes the following boundary conditions:
  (i) isotropic background radiation,
  (ii) any desired temperature distribution,
  (iii) transparent or opaque boundaries,
  (iv) diffuse, specular, or black walls,
  (v) boundaries can be planes of symmetry, and
  (vi) periodic boundaries.
(7) Sources: the model allows for any distribution of internal energy sources.
(8) Interfacing: the model can be interfaced with existing codes that solve for other forms of energy transfer.
(9) Radiative equilibrium: the model is able to solve for radiative equilibrium.
(10) Output: the outputs of the model are:
  (i) heat fluxes along all the boundaries,
  (ii) intensity field,
  (iii) divergence of the radiative heat flux vector (on a grid by grid basis),
  (iv) temperature distribution in cases involving radiative equilibrium, and
  (v) outgoing intensity in any given direction (sensor).
(11) Grid: the algorithm supports uniform or non uniform grid.
(12) Numerical characteristics: the model is accurate and stable.

The model has been successfully bench marked against available solutions in one-, two- and three-dimensional geometries including isotropic and anisotropic participating media; homogeneous and nonhomogeneous media; optically thin and optically thick atmospheres; internal sources; parallel beam and sensor at varied polar and azimuthal angles; radiative equilibrium; black, gray, and highly reflecting walls; spectrally participating media and walls; and practically all types of boundary conditions. Furthermore, the capabilities of the model have been exemplified with the solution of problems that included interfacing with existing codes solving for other forms of energy transfer (including natural and forced convection); three-dimensional collimated source and sensor configurations at different angles and under different scattering conditions; three-dimensional nonhomogeneous problems in optically thin and optically thick settings; and three-

dimensional spectral problems including spectral equilibrium. Although these results cannot, in general, be validated against the results of other studies, both physical and qualitative arguments indicate that the answers obtained from the model are plausible.

The performance of the model in the evaluation of the radiative properties of particles and polydispersions as well as for theoretical phase functions has been verified. The usefulness of the modified δ–M scaling technique in the treatment of problems involving large optical thicknesses and highly scattering media has also been evidenced.

The model is applied to simulate radiative transfer in a broken cloud field. The results obtained point to the importance of the three-dimensional aspects of radiative transfer modeling. This has serious implications for the interpretation of remote sensing images of clouds and estimation of rainfall.

The authors have extended this study to examine three-dimensional aspects of raining clouds over a reflecting surface (Haferman et al., 1993). The model is being applied to simulate microwave observations of the COHMEX storm, much like Mugnai et al. (1990) who used a one-dimensional radiative transfer model.

Acknowledgments

The authors wish to acknowledge partial support for this study from the grant NA89AA-D-AC195, National Oceanic and Atmospheric Administration: Global Change Program. The senior author (A.S.) would also like to recognize the financial support received from Universidad de los Andes and Fundación Gran Mariscal de Ayacucho, both of the Republic of Venezuela.

References

Adler, R.F., Yeh, H.-Y.M., Prasad, N., Tao, W.-K. and Simpson, J., 1991. Microwave simulations of a tropical rainfall system with a three-dimensional cloud model. J. Appl. Meteorol., 30: 924–953.

Bohren, C.F. and Huffman, D.R., 1983. Absorption and Scattering of Light by Small Particles. Wiley, New York, 530 pp.

Carlson, B.G. and Lathrop, K.D., 1968. Transport theory, the method of discrete-ordinates. In: H. Greenspan, C.N. Kelber and D. Okrent (Editors), Computing Methods in Reactor Physics. Gordon and Breach, New York, pp. 171–266.

Crosbie, A.L. and Schrenker, R.G., 1985. Multiple scattering in a two-dimensional rectangular medium exposed to collimated radiation. J. Quant. Spectrosc. Radiat. Transfer, 33: 101–125.

Deirmendjian, D., 1964. Scattering and polarization of water clouds and hazes in the visible and infrared. Appl. Opt., 3: 187–196.

DOE, 1990a. Atmospheric Radiation Measurement Program, DOE/ER-0441, U.S. Dept. of Energy. Washington, DC.

DOE, 1990b. Executive Summary: Atmospheric Radiation Measurement Program, DOE/ER-0442, U.S. Dept. of Energy. Washington, DC.

Fiveland, W.A., 1988. Three-dimensional radiative heat transfer solutions by the discrete-ordinates method. J. Thermophys. Heat Transfer, 2: 309–316.

Fiveland, W.A., 1991. The selection of discrete ordinate quadrature sets for anisotropic scattering. In:

W.A. Fiveland, A.L. Crosbie, A.M. Smith and T.F. Smith (Editors), Fundamentals of Radiation Heat Transfer. Am. Soc. Meteorol. Eng., HTD, 160: 89–96.

Fiveland, W.A. and Jamaluddin, A.S., 1991. Three-dimensional spectral heat transfer solutions by the discrete-ordinates method. J. Thermophys. Heat Transfer, 5: 335–339.

Fu, Q. and Liou, K.N., 1992. On the correlated k-distribution method for radiative transfer in non-homogeneous atmospheres. J. Atmos. Sci., 49: 2139–2156.

Gerstl, S.A.W. and Zardecki, A., 1985. Discrete-ordinates finite-element method for atmospheric radiative transfer and remote sensing. Appl. Opt., 24: 81–93.

Haferman, J.L., Krajewski, W.F., Smith, T.F. and Sánchez, A., 1993. Radiative transfer for a three-dimensional raining cloud. Appl. Opt., 32: 2795–2802.

Jamaluddin, A.S. and Smith, P.J., 1988. Predicting radiative transfer in rectangular enclosures using the discrete ordinates method. Combust. Sci. Technol., 59: 321–340.

Kim, T.K. and Lee, H.S., 1989. Radiative transfer in two-dimensional anisotropic scattering media with collimated incidence. J. Quant. Spectrosc. Radiat. Transfer, 42: 225–238.

Kim, T.K. and Lee, H.S., 1990a. Scaled isotropic results for two-dimensional anisotropic scattering media. J. Heat Transfer, 112: 721–727.

Kim, T.K. and Lee, H.S., 1990b. Modified δ–M scaling results for mie-anisotropic scattering media. J. Heat Transfer, 112: 988–994.

Kim, T.K., Menart, J.A. and Lee, H.S., 1991. Nongray radiative analysis using the S–N discrete ordinates method. J. Heat Transfer, 113: 946–952.

Kobayashi, T., 1989. Radiative properties of finite cloud fields over a reflecting surface. J. Atmos. Sci., 46: 2208–2214.

Lenoble, J., 1985. Radiative Transfer in Scattering and Absorbing Atmospheres: Standard Computational Procedures. A. Deepak, Virginia.

Mandelbrot, B.B., 1983. The Fractal Geometry of Nature. Freeman, New York.

McKee, T.B. and Cox, S.K., 1976. Simulated radiances for finite cubic clouds. J. Atmos. Sci., 33: 2014–2020.

Menguc, M.P. and Viskanta, R., 1985. Radiative transfer in three dimensional rectangular enclosures containing nonhomogeneous, anisotropic scattering media. J. Quant. Spectrosc. Radiat. Transfer, 33: 533–549.

Mugnai, A., Cooper, H.J., Smith, E.A. and Tripoli, G.J., 1990. Simulation of microwave brightness temperatures of an evolving hailstorm at SSM/I frequencies. Bull. Am. Meteorol. Soc., 71: 2–13.

Naraghi, M.H.N. and Huan, J., 1991. An N-bounce method for analysis of radiative transfer in enclosures with anisotropically scattering media. J. Heat Transfer, 113: 774–777.

Naraghi, M.H.N., Chung, B.T.F. and Litkouhi, B., 1988. A Continuous exchange factor method for radiative exchange in enclosures with participating Media. J. Heat Transfer, 110: 456–462.

Sánchez, A., 1991. A general purpose radiative transfer model for application to remote sensing in multi-dimensional systems. Ph.D. Thesis, Dept. of Mechanical Engineering, The University of Iowa, Iowa City, IA.

Sánchez, A. and Smith, T.F., 1992. Surface radiation exchange for two-dimensional rectangular enclosures using the discrete-ordinates method. J. Heat Transfer, 114: 465–472.

Sánchez, A., Krajewski, W.F. and Smith, T.F., 1992. A general radiative transfer model for atmospheric remote sensing studies in multi-dimensional media. Tech. Rep. No. 355, Iowa Inst. of Hydraulic Res., The University of Iowa, Iowa City, IA.

Sánchez, A., Smith, T.F. and Krajewski, W.F., 1993. Dimensionality issues in modeling with the discrete-ordinates method. J. Heat Transfer, in press.

Simpson, J., Adler, R.F. and North, G., 1988. A proposed tropical rainfall measuring mission (TRMM) satellite. Bull. Am. Meteorol. Soc., 69: 278–295.

Stephens, G.L., 1988. Radiative transfer through arbitrarily shaped optical media. Part I: A general method of solution. J. Atmos. Sci., 45: 1818–1836.

Tan, Z. and Howell, J.R., 1990. Two-dimensional radiative heat transfer in an absorbing, emitting, and linearly anisotropically scattering medium exposed to a collimated source. In: T.F. Smith, M.F. Modest, A.M. Smith, S.T. Thynell (Editors), Radiation Heat Transfer: Fundamentals and Applications. Am. Soc. Meteorol. Eng., HTD, 137: 101–106.

Truelove, J.S., 1988. Three-dimensional radiation in absorbing–emitting–scattering media using the discrete-ordinate approximation. J. Quant. Spectrosc. Radiat. Transfer, 39: 27–31.
Welch, R.M. and Wielicki, B.A., 1989. Reflected fluxes for broken clouds over a Lambertian surface. J. Atmos. Sci., 46: 1384–1395.
Wiscombe, W.J., 1977. The Delta-M method: rapid yet accurate radiative flux calculations for strongly asymmetric phase functions. J. Atmos. Sci., 34: 1408–1442.